

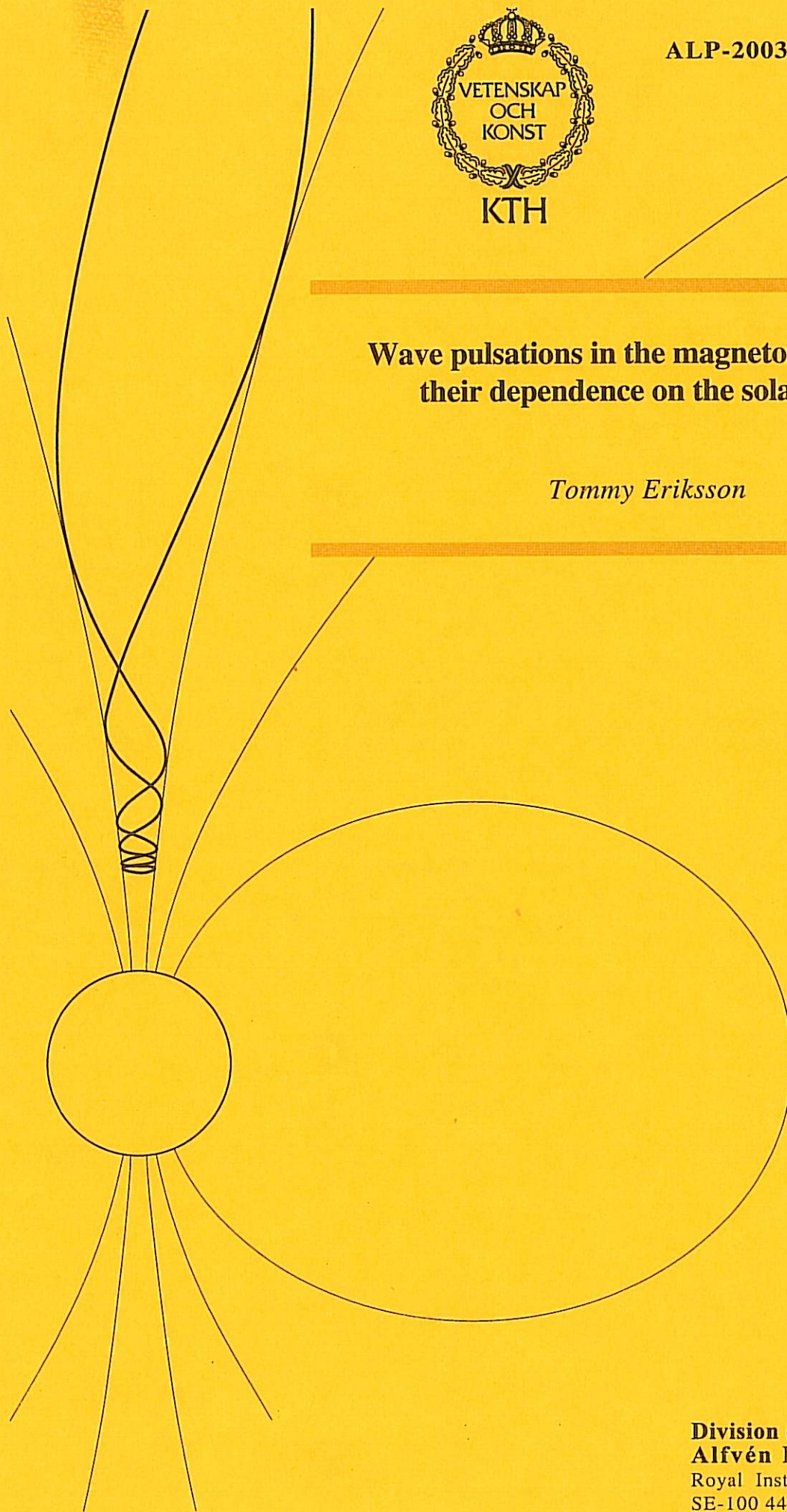


KTH

ALP-2003-101

Wave pulsations in the magnetosphere and their dependence on the solar wind

Tommy Eriksson



**Division of Plasma Physics
Alfvén Laboratory**
Royal Institute of Technology
SE-100 44 Stockholm, Sweden

Wave pulsations in the magnetosphere and their
dependence on the solar wind

Tommy Eriksson

Abstract

A study of coherent MHD waves in the solar wind as a possible source mechanism for Pc-5 pulsation has been performed. Solar wind data from the ACE satellite have been correlated with data from the SHARE HF radar on Antarctica. In a number of events the pulsations showed good correspondence with waves in the solar wind. The frequency band $0.8 - 1.2$ mHz showed an especially good correlation. These frequencies are otherwise hard to explain with the current theoretical model.

Sammanfattning

En studie över huruvida koherenta MHD-vågor i solvinden kan driva Pc-5-pulsationer har genomförts. Solvindsdata från ACE har korrelerats med data från SHARE HF radar på Antarktis. Vid ett flertal tillfällen uppvisar pulsationerna god överensstämmelse med vågor i solvinden. Speciellt syns en extra god korrelation för frekvensbandet $0.8 - 1.2$ mHz. Dessa frekvenser är annars svåra att förklara med den rådande teoretiska modellen.

Contents

1	Introducing the physics	2
1.1	The plasma state and magnetohydrodynamics	2
1.2	The solar wind	3
1.3	The bow shock	4
1.4	The magnetosphere	4
1.5	The ionosphere	5
2	Field line resonances and a possible source mechanism	7
2.1	Ultra low frequency fluctuations in the geomagnetic field	7
2.2	A model for the excitation of Pc-5 pulsation by MHD waves originating in the solar wind	8
3	Instrumentation	9
3.1	Instruments used	9
3.1.1	The ACE satellite	9
3.1.2	The SHARE SuperDARN HF Radar at Vesleskarvet	10
3.1.3	The WIND satellite	10
4	Data Analysis	13
4.1	Finding good data	13
4.2	Comparing the two signals	13
4.2.1	The analytic signal	15
4.2.2	Cross-correlation	16
4.3	Summary of the data analysis	17
5	Results	18
5.1	Studied events	18
5.2	Presentation of data and plots	18
5.3	Some results regarding the spatial structure of the solar wind	28
6	Discussion and Conclusions	31
6.1	Main conclusions	31
6.2	Discussion	31
6.3	Future directions	32

Chapter 1

Introducing the physics

1.1 The plasma state and magnetohydrodynamics

A plasma can be defined as an ionised gas with some additional properties. One is *quasi-neutrality*, which means that the density of positive and negative charges is nearly equal. A parameter very closely linked to quasi-neutrality is the *Debye length* λ_D . This parameter can be derived as follows: In an ionised gas with electron density n_e assume that the electrons have been displaced a distance Δx from the positive particles. This creates an electrostatic potential according to Poisson's equation. The potential energy difference for an electron over Δx is then

$$\Delta W = \frac{e^2 n_e (\Delta x)^2}{2\epsilon_0} \quad (1.1)$$

Now the largest potential gap that can be maintained is determined by the kinetic energy of the electrons which is $kT_e/2$. So if we assume that these two energies are equal we get an expression for this largest potential gap and this is the Debye length

$$\lambda_D \equiv \Delta x = \sqrt{\frac{\epsilon_0 k T_e}{e^2 n_e}} \quad (1.2)$$

The Debye length is a measure of the largest distance where a charge imbalance can be maintained. For an ionised gas to be called a plasma it is usually required that its characteristic length l_c must be much larger than λ_D .

In theory it would be possible to write down equations of motion for each individual particle. However the number of particles involved in almost every plasma phenomenon is enormous, which makes it impossible to solve the equations in practise. One way to overcome this difficulty is to regard the plasma as a continuum (i.e., a fluid). This means that we get one equation of motion for the entire plasma. The most common one-fluid model is the *magnetohydrodynamic* (MHD) model. This model incorporates the four Maxwell equations (since there are charged particles involved):

$$\nabla \times \mathbf{E} = -\frac{\partial \mathbf{B}}{\partial t} \quad (\text{Faraday's law}) \quad (1.3)$$

$$\nabla \times \mathbf{H} = \mathbf{j} + \frac{\partial \mathbf{D}}{\partial t} \quad (\text{Ampère's law}) \quad (1.4)$$

$$\nabla \cdot \mathbf{D} = \rho \quad (\text{Gauss' law}) \quad (1.5)$$

$$\nabla \cdot \mathbf{B} = 0 \quad (\text{No magnetic monopoles}) \quad (1.6)$$

the equation of motion (which can be obtained by regarding the plasma distribution function in the phase space)

$$\rho \frac{d\mathbf{v}}{dt} = \mathbf{i} \times \mathbf{B} - \nabla p \quad (1.7)$$

Ohm's law and the continuity equation.

$$\mathbf{i} = \sigma(\mathbf{E} + \mathbf{v} \times \mathbf{B}) \quad (1.8)$$

$$\frac{\partial \rho}{\partial t} + \nabla \cdot (\rho \mathbf{v}) = 0 \quad (1.9)$$

These equations can be linearised and combined to obtain a wave equation (the displacement current in 1.4 is usually very small in most plasmas and can thus be neglected). This was first done by Hannes Alfvén in 1942 and the resulting waves are called *Alfvén waves*. These waves propagate with a phase speed $V_A = B/\sqrt{\mu_0 \rho}$ called the *Alfvén speed*.

In this derivation it has been assumed that the fluid is incompressible ($\nabla \cdot \mathbf{v} = 0$, $\rho = \text{const.}$). If the dynamic pressure of the system is comparable to the magnetic pressure (i.e., it can not be omitted), then one more equation is needed. This equation states that the specific entropy is conserved in the convecting plasma:

$$\left(\frac{\partial}{\partial t} + \mathbf{u} \cdot \nabla \right) \left(\frac{p}{\rho^\gamma} \right) = 0 \quad (1.10)$$

The Alfvén waves are then not the only solution to the obtained wave equation, there also exists two other wave modes, called the *fast and slow magnetoacoustic wave*. In general, waves in a magnetohydrodynamic media are called magnetohydrodynamic waves.

1.2 The solar wind

The Sun does not only emit electromagnetic waves but also radiates particles. This particle radiation (or plasma flow), called the solar wind, mainly consists of protons, alpha particles and electrons in equal proportions. The outflow is a result of a pressure imbalance between the hot corona (over 2 million degrees) and the cold, tenuous interstellar gas. The flow starts with a low outward velocity, accelerates through the corona and reaches sonic speed at about 4 to 6 solar radii from the Sun's centre. It thereafter becomes supersonic (and super-Alfvénic) and flows with a speed of 300 - 900 km/s.

A well known result from plasma physics is that when the magnetic Reynolds number R_m

$$R_m = \mu_0 \cdot \sigma \cdot l_c \cdot v_c \quad (1.11)$$

Proton density	6.6 cm ³
Electron density	7.1 cm ³
Flow speed	450 kms ⁻¹
Proton temperature	1.2 · 10 ⁵ K
Electron temperature	10 ⁵ K
Magnetic field	7 nT

Table 1.1: Typical values of the Solar wind (From Kivelson and Russel 1995).

is much greater than unity, the magnetic field lines becomes frozen-in in the plasma (l_c is the characteristic length of the observed system). This can be seen as follows: If a magnetic field line connects two elements of the plasma at a given time, a field line will still connect the two elements at any other given time independently of the relative motion between the two elements. For most practical considerations the criterion is by far fulfilled in the solar wind. Table (1.1) shows some typical data for the solar wind at a distance of 1 AU from the Sun.

1.3 The bow shock

When the solar wind reaches the Earth's magnetosphere, which in this case acts like an obstacle, a bow shock is formed where the plasma is slowed down to subsonic speed. Shocks occur whenever an object travels with supersonic speed through a medium (e.g., an aircraft), but what is extraordinary with the bow shock is that it is collisionless (i.e., the contribution from binary collisions can be neglected). This is due to the fact that the mean free path in the solar wind is about 1 AU and the thickness of the bow shocks is only 100 - 1000 km. The shock is curve-shaped and symmetrical with respect to the Sun - Earth line. Its most sunward part is located at about 14 earth radii from the centre of the Earth. The distance to the magnetosphere (see section 1.4), called the *stand-off distance*, is a few Earth radii. Its average shape in the equatorial plane can be calculated from the formula

$$\frac{23.3}{R} = 1 + 1.16 \sin \theta \quad (1.12)$$

where R is measured in R_E and θ is the angle from the Sun - Earth line. Behind the bow shock there is a region of subsonically flowing plasma which is called the magnetosheath.

1.4 The magnetosphere

The magnetosphere is the region in space where the Earth's magnetic field is dominant. Without any external influence the geomagnetic field would almost be a dipole field, but since the solar wind is present it becomes deformed. Its shape is shown in figure 1.1.

The magnetosphere can be divided into many different regions, each containing a plasma population of varying temperature and density. The outermost part is the magnetopause which borders to the magnetosheath. This is where the

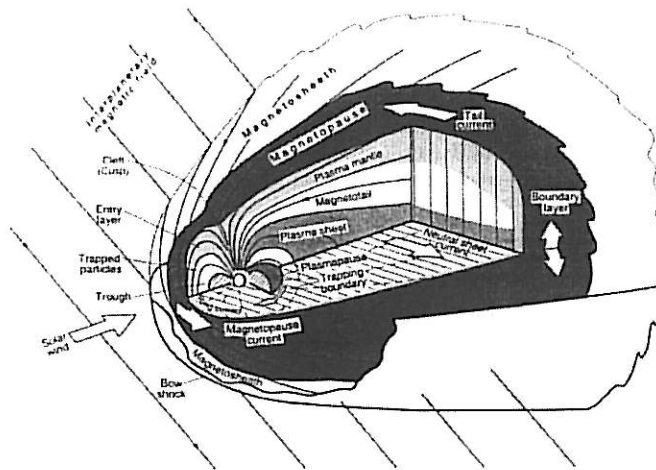


Figure 1.1: The structure of the magnetosphere.

boundary between the Earth's magnetic field and the interplanetary magnetic field is situated. Often this is seen as a sudden change in the field direction. Originally the magnetopause was called the *Cahill discontinuity*. Along the magnetopause flows an eastward current called the *Chapman - Ferraro Current*. The location of the magnetopause is determined by the pressure balance between the solar wind's dynamic pressure $p_d = \rho_m v^2$ (ρ_m being the density of the wind and v its flow speed), and the magnetic pressure of the geomagnetic field $B^2/2\mu_0$. Because of the dynamic nature of the solar wind this distance normally varies between 8 - 12 Earth radii, but can sometimes be as small as 6.6 Earth radii and hereby affecting satellites in the geostationary orbit, which are located at this distance.

Close to the Earth is a relatively dense plasma population called the *plasmasphere*. It can be seen as a continuation of the Earth's ionosphere (see section 1.5). The temperature of the plasma is some thousands of K and the density is about $10\text{-}100\text{ cm}^{-3}$. Due to the good coupling to the ionosphere, the plasmasphere corotates with the Earth. Its outer boundary is called the *plasmapause*. Outside the plasmapause, on the dayside, there is a region of low density called the *trough*.

1.5 The ionosphere

The ionosphere is the electrically conductive part of the Earth's atmosphere. The ionisation is due to high-energy radiation from the Sun (mainly soft x-ray and uv-light) and cosmical particle radiation. It ranges from about 70 km to 1500 km in altitude. Usually a distinction of four different layers, D, E, F1 and F2, is made. This substructure of the ionosphere is due to the fact that

the atmosphere consists of several different gases which are ionised at different altitudes. The night-time ionosphere differs from the daytime simply because the type of ionising radiation in the daytime is different from that in the night-time.

Chapter 2

Field line resonances and a possible source mechanism

2.1 Ultra low frequency fluctuations in the geomagnetic field

Rapid variations in the geomagnetic field are called magnetic pulsations. These pulsations can either be continuous, in which they are called Pc pulsation, or irregular, called Pi pulsations. The pulsations are further categorised into different frequency ranges as seen in Table (2.1). The first observations of these pulsations were made on the ground by Stewart 1861, but it was not until 1954 that Dungey suggested that MHD waves in the magnetosphere were the source of the measured fluctuations in the magnetic field. The MHD waves propagate along the magnetic field lines and are reflected at the ionosphere due to its high conductivity. The waves can only satisfy the boundary conditions at the ionosphere for certain wavelengths. This gives a requirement on the wavelength of the wave. If the length of the magnetic field line between the two turning points at the ionosphere is l , then the allowed wavelengths are $\lambda = 2l/n$, where n is an integer. If λ fulfils this condition the result is called a field line resonance (FLR). Here we will direct our attention to the Pc-5 pulsations.

The Pc-5 pulsations have been observed [Samson *et al.*, 1991 and Rouhoniemi *et al.*, 1991] to occur at certain favoured frequencies: 1.3, 1.9, 2.6 and 3.3 mHz. The source (or sources) of the Pc-5 pulsations is still a matter of debate. The first theory [Southwood, 1974; Chen and Hasegawa, 1974] was that Kelvin - Helmholtz instability at the magnetopause, driven by the streaming magnetosheath plasma, produces surface waves (cf., the waves on a lake when the wind is blowing). These surface waves create compressions in the magneto-

	Pc-1	Pc-2	Pc-3	Pc-4	Pc-5	Pi-1	Pi-2
T(s)	0.2-5	5-10	10-45	45-150	150-600	1-40	40-150
f	0.2-5 Hz	0.1-0.2 Hz	22-100 mHz	7-22 mHz	2-7 mHz	0.025-1 Hz	2-25 mHz

Table 2.1: Classification of ULF fluctuations (From Kivelson and Russel 1995)

sphere and thus compressional waves (fast waves). The compressional waves can propagate across the geomagnetic field lines in the magnetosphere and excite shear Alfvén waves at the location where the wavelength matches the length of the local magnetic field line (as described above). This theory has the flaw that it does not explain the predominant frequencies of the resonances.

Another model focuses on the idea of the magnetosphere acting as a resonant cavity (bounded by the near-equatorial ionosphere and the magnetopause). Abrupt changes in the solar wind's dynamic pressure could excite compressional waves matching the frequencies of the cavity, i.e., the frequencies of the compressional waves will be quantified. This compressional wave then excites a field line resonance in the same way as in the first theory.

2.2 A model for the excitation of Pc-5 pulsation by MHD waves originating in the solar wind

Walker (2002) recently suggested that Pc-5 pulsations may be driven directly by MHD waves in the solar wind. The MHD waves have to propagate through the bow shock and the magnetosheath. However only the compressional (fast) wave is able to propagate through both the bow shock and the magnetosheath, so it is assumed that it is a compressional wave that is incident on the bow shock.

Inside the magnetopause wave propagation is possible, and as the Alfvén speed increases with decreasing radius a turning point is reached where the waves are reflected. The location of the turning point is of course dependent of the frequency of the wave. Thus there is a cavity or waveguide formed by the turning point and the magnetopause. There is in general a mismatch between the magnetopause and the magnetosphere so that the wave is almost entirely reflected at the magnetopause. However, if the frequency of the incident wave matches the natural frequency of the cavity, the wave is captured in the cavity. This condition can also be formulated such that the total phase change between the two boundaries of the cavity must be an integral multiple of 2π . Once inside the cavity the wave can leak energy through evanescent barrier penetration, that is, although the wave is damped a considerable amount of energy can propagate through since the evanescent region is much smaller than a wavelength of the wave. This energy can then excite a field line resonance.

Chapter 3

Instrumentation

3.1 Instruments used

One of the objectives of this thesis is to establish whether coherent MHD waves in the solar wind excite field line resonances. These field line resonances, or rather the effect of them, can be measured by ground based magnetometers or by strategically placed High Frequency (HF) radars. Here the attention is directed at the radars since they give a much better spatial resolution than the magnetometers. Another advantage of the radars is that they have a better spatial coverage. The solar wind waves of course have to be measured *in situ*. This is done by a satellite placed in the upstream solar wind.

All times are given in Universal Time (UT).

3.1.1 The ACE satellite

The Advanced Composition Explorer (ACE) is located at about $200 R_E$ upstream from Earth. Its orbit is approximately a circle around the Sun-Earth line (i.e., the x-axis in GSE coordinates). This ephemeris makes ACE a good instrument for measuring waves in the solar wind that will later “hit” the magnetosphere. The satellite contains instruments for measuring solar wind plasma parameters such as: The solar wind proton number density and the solar wind velocity. These parameters are needed to calculate the dynamic pressure of the solar wind. In this thesis only the first order quantity of the solar wind dynamic pressure is considered, i.e., the density of the solar wind plasma ρ is taken as a zeroth order term. Thus the dynamic pressure is given by the formula

$$p_{dyn} = \frac{1}{2} \rho_0 (v_{wind})^2 \quad (3.1)$$

Where v_{wind} is the absolute value of the solar wind velocity. The zeroth order term ρ_0 is calculated by taking an average of the density data from ACE for the time sequence used. The data used from ACE are level 2 data with a time resolution of 64 seconds.

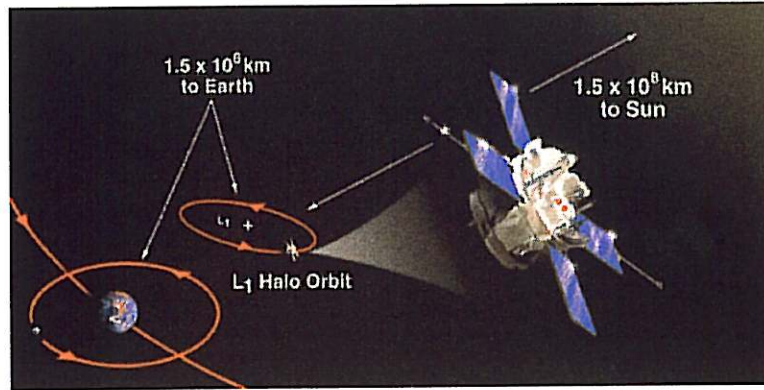


Figure 3.1: ACE and its orbit at L1.

3.1.2 The SHARE SuperDARN HF Radar at Vesleskarvet

The Super Dual Auroral Radar Network [Greenwald *et al.*, 1993] consists, at present (November 2002), of 16 radars, 10 of which are located in the northern hemisphere and 6 in the southern hemisphere. Each radar consists of 16 log-periodic antennas. Electronically controlled time-delay phasing elements are used to steer signals to or from the radar into 16 different directions (or beams). Each beam is divided into range bins (or range gates). These radars are sensitive to electron irregularities in the E- and F-regions of the ionosphere. The irregularities cause the radar signal to backscatter and if the signal is propagating perpendicular to the magnetic field at the time of backscatter, the signal will come back to the radar. For the SuperDARN radars the backscatter is assumed to occur at 300 km (altitude).

The SHARE radar is located at Vesleskarvet, Antarctica (71,1°S, 2,8°W). For this study only beam 4 has been used. This beam makes a small angle with lines of constant L, and since FLRs oscillate perpendicular to the magnetic meridian a large component of this oscillation is therefore seen with this beam. The radar operates in different “scanning” modes, the most common ones being the normal scan mode and the high normal scan mode. In the normal mode the scan is carried out in an orderly fashion through every beam, dwelling 7 seconds in each. This is repeated every two minutes. For the high normal mode the dwell time is 3 seconds in each beam and the cycle is repeated every 60 seconds. The remaining time in every cycle is used for “house-keeping.” A sample rate of two minutes may seem low but since the Pc-5 pulsation have periods of several minutes it is adequate for this analysis. Of course, a higher sampling rate is better and as many events as possible where the radar operated in the high scan mode have been used.

3.1.3 The WIND satellite

WIND has (like ACE) instruments for measuring various solar wind parameters. However, WIND’s orbit does not make it suitable for the solar wind - FLR correlation analysis performed in this thesis since its more or less “all over the

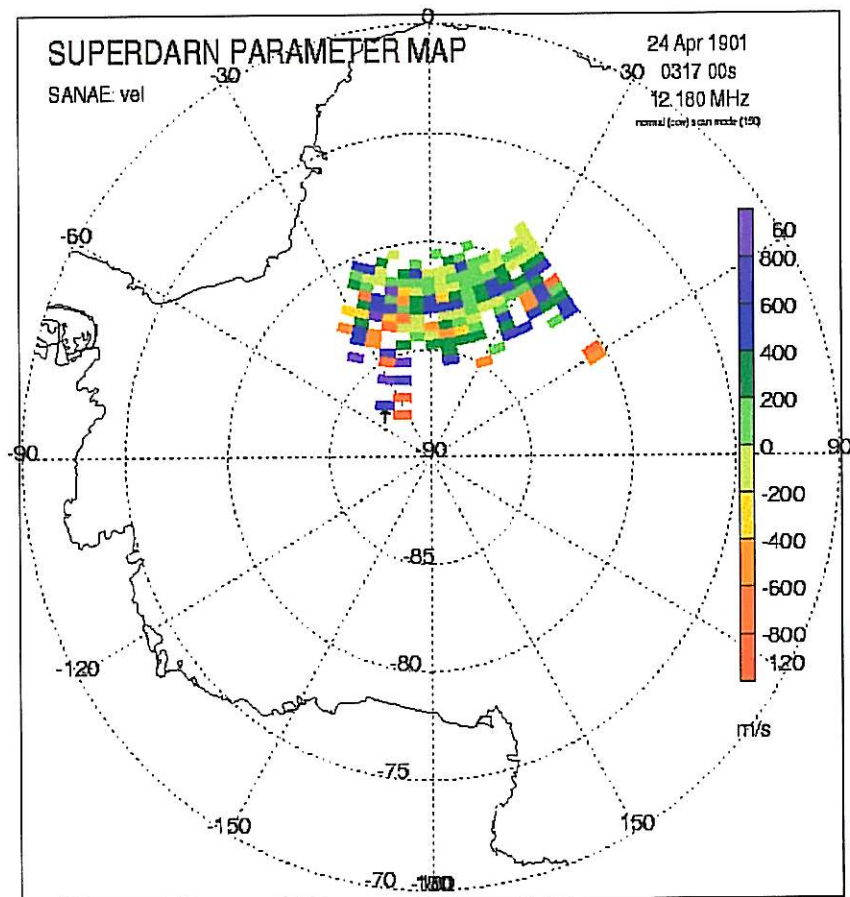


Figure 3.2: Typical area of backscatter from the SHARE radar. The solid line is the Antarctic coast line. The geographic south pole is located at the centre of the plot. The beams are aligned with beam 1 to the far left and beam 16 to the far right. Beam 4 is indicated by the arrow. (The date should of course be 24 Apr 2001.)

place."Instead WIND has been used to look at the spatial structure of the solar wind incident on Earth. This is done by correlating data from WIND with ACE data. The solar parameter sample rate is higher than the 64 second sample rate of ACE and also varying over time making it more troublesome comparing its data with ACE data.

Chapter 4

Data Analysis

4.1 Finding good data

The analysis starts by looking at SuperDARN summary plots (see figure 4.1), to find an event where there is at least an hour of consecutive backscatter. This amount of time is needed to see the wavepacket structure of the FLRs, since the lowest frequencies considered have periods longer than 10 minutes. For the normal scan mode of the radar a longer time is needed than for the high scan mode.

Once a good sequence is identified the data are averaged over three/four range gates for high/normal scan mode respectively. In this manner, single missing data points will be smoothed over and a longer uninterrupted data sequence can be obtained. This process does not distort the data since adjacent range bins tend to have similar values for the doppler velocity.

The data sequence from ACE is chosen so that it has the same length as the radar data sequence but it precedes the latter with about the travel time for the solar wind from the ACE position to the magnetosphere. Single missing data points in the ACE data are replaced by the average of its preceding and superseding values. This again is done in order to get a longer time sequence, since missing data points are not that uncommon. If a sequence of missing data points occur however, nothing much can be done and the sequence has to be omitted.

4.2 Comparing the two signals

The response of the magnetosphere to a given input signal is immensely complicated, making a direct comparison between solar wind and radar data a futile exercise. Filtering and other means of processing are thus needed. Another problem that arises is the discrepancy in sample rate between ACE and the radar. This is dealt with by pointwise linear interpolation of the ACE data so that it matches the sample rate of the radar. Although this introduces an error, this error is likely to be small in comparison to other distorting mechanisms affecting the signal as it propagates through the magnetosphere. One objection

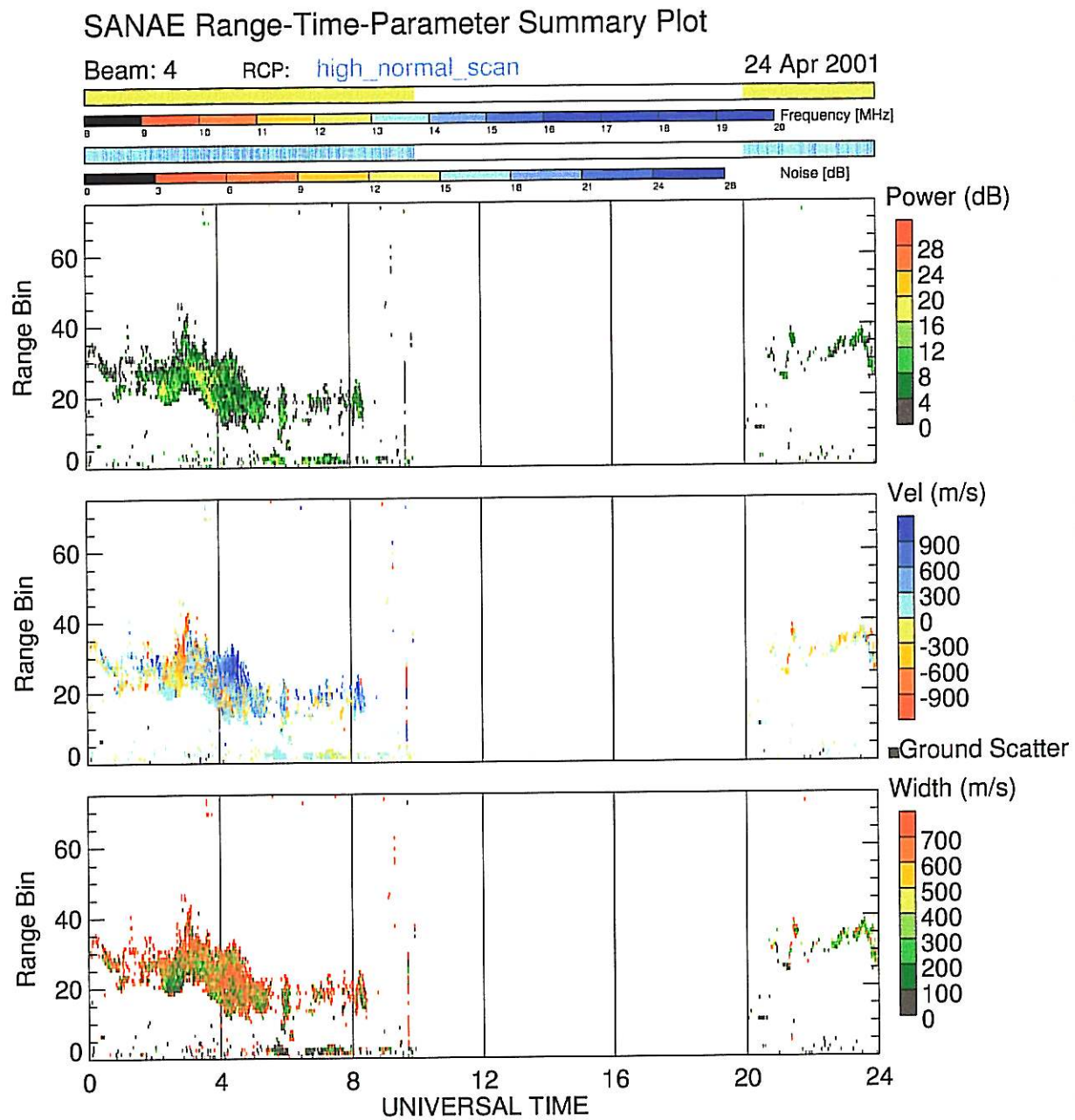


Figure 4.1: SuperDARN summary plot for the HF radar at SANA E. Good backscatter, and signs of pulsations, are seen between 02:00 and 06:00 UT.

that could be made to this is that a higher order interpolation should be better, but since there really is no way of knowing the value of the signal between two samples and thus the error in the interpolation, it is argued that the simplest estimate is as good as any.

To compare both of the signals in the frequency domain they are Fourier transformed using the discrete Fourier transform (DFT). For an N-element function $f(x)$ this is defined as

$$F(u) = \frac{1}{N} \sum_{x=0}^{N-1} f(x) \exp(-2\pi i u x / N) \quad (4.1)$$

and the inverse as

$$f(x) = \sum_{u=0}^{N-1} F(u) \exp(2\pi i u x / N) \quad (4.2)$$

Also a Hanning window is applied in order to reduce the "smearing" effect due to the definition of the DFT. Both sets of power spectra are normalised with their maximum value respectively.

In order to study the FLRs more closely and compare them with the solar wind signal a bandpass filter has been used. This filter is implemented by the DFT and filtering is done in the frequency domain. The reason for this is that it has been found that filtering in the time domain (i.e., by convolving the filter with the signal) is far less accurate, mainly due to the relatively small number of data points (the order of a hundred). The width of the filters implemented has been taken as small as possible and is between 0.3-0.6 mHz. No Hanning window is used in the filter implementation.

4.2.1 The analytic signal

The analytic signal is a good tool for studying monochromatic signals. This is achieved by using some of the many pleasant properties of the Hilbert transform. The analytic signal $A(t)$ for a time signal $f(t)$ is given by

$$A(t) = f(t) - iF(t) \quad (4.3)$$

Where $F(t)$ is the Hilbert transform of $f(t)$ defined in the usual manner:

$$F(t) = \frac{1}{\pi} \int_{-\infty}^{\infty} \frac{f(x)}{x - t} dx \quad (4.4)$$

The analytic signal is thus a phasor in the complex plane. For instance the analytic signal for $\cos \omega t$ is $e^{i\omega t}$ and the corresponding signal for $\sin \omega t$ is $ie^{i\omega t}$.

Here the Hilbert transform is constructed as follows:

The DFT of the signal is computed, the resulting positive/negative frequency components are multiplied by $i/-i$ respectively. The constant elements in the transform are not changed. The resulting vector is then inverse transformed using 4.2.

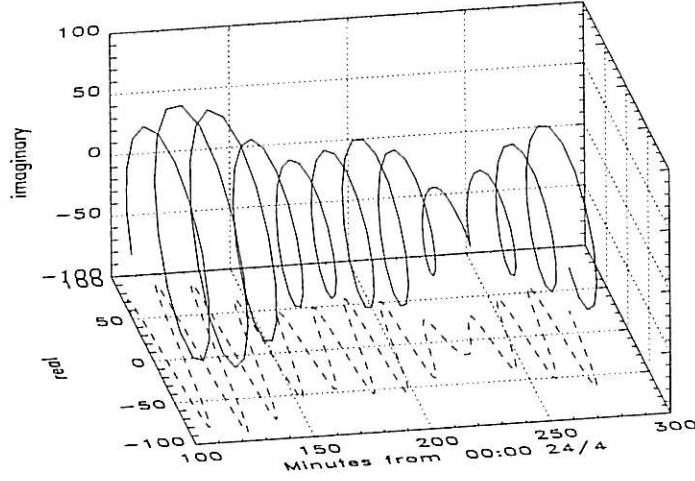


Figure 4.2: The analytic signal constructed from bandpass filtered (1.3-1.7 mHz) SHARE HF radar data. The dashed line is the real part of the analytic signal (i.e., $f(t)$ in equation 4.3).

From the analytic signal the amplitude and phase of the signal can be extracted. The phase can in turn be used to calculate the instantaneous frequency. Information about the amplitude is useful for studying the wave-packet structure of both the FLRs (e.g., Walker *et al.*, 1992) and the coherent MHD waves in the solar wind. An example of an analytic signal is shown in figure 4.2.

4.2.2 Cross-correlation

To see if the observed wave packet structure of the FLRs is similar to that of the solar wind pressure a cross-correlation is performed. The correlation coefficient is a measure of the linear dependence between two signals. For two discrete sample populations, $x = (x_0, x_1, x_2, \dots, x_{N-1})$ and $y = (y_0, y_1, y_2, \dots, y_{N-1})$, it is given by the formula

$$P_{xy}(L) = \begin{cases} \frac{\sum_{k=0}^{N+L-1} (x_{k-L} - \bar{x})(y_k - \bar{y})}{\sqrt{\left[\sum_{k=0}^{N-1} (x_k - \bar{x})^2 \right] \left[\sum_{k=0}^{N-1} (y_k - \bar{y})^2 \right]}} & \text{For } L < 0 \\ \frac{\sum_{k=0}^{N-L-1} (x_k - \bar{x})(y_{k+L} - \bar{y})}{\sqrt{\left[\sum_{k=0}^{N-1} (x_k - \bar{x})^2 \right] \left[\sum_{k=0}^{N-1} (y_k - \bar{y})^2 \right]}} & \text{For } L \geq 0 \end{cases} \quad (4.5)$$

Where \bar{x} and \bar{y} are the mean of x and y respectively. From this the correlation coefficient is computed for a sequence of lag-times. This yields a plot that gives a qualitative estimate of how well the two signals correspond to each other, and

at what time this correspondence (if it exists) has a maximum. Notice that the doppler velocity signal is taken to start at about the travel time of a fast MHD wave (from ACE to the position of the FLR) later then the pressure signal. This means that for $L = 0$ in formula 4.5 it is the correlation for this time lag that is being computed. So that the lag displayed in the correlation plots is $L + \Delta t$, where Δt is the difference between the start time for the radar data and the start time for the satellite data. When correlating ACE and WIND data no time shifts are applied to the data, meaning that in this case the lag displayed in the plots is identical to L in formula 4.5.

4.3 Summary of the data analysis

- An event where at least an hour of consecutive backscatter exists is selected and a radar data vector is extracted.
- The propagation time for the solar wind to the magnetopause is calculated and the start time for the ACE data vector is selected accordingly.
- The dynamic pressure is computed from formula 3.1. The pressure data are then processed using pointwise linear interpolation to match the radar sample rate (60 or 120 seconds depending on the scan mode).
- The spectrum is calculated for both sets of data and normalised with their highest value respectively. Both spectra are then plotted in the same plot.
- Four interesting frequency bands are selected. These frequency bands are filtered out and the analytic signal is calculated for each band. This gives four pairs of signals where the correlation for each pair is to be determined.
- From the analytic signal the envelope for each band is given and used to compute the correlation coefficient.

Chapter 5

Results

5.1 Studied events

Ten different events (days) have been studied and are summarised in table 5.1. Depending on the amount of available backscatter two or three different sets of range gates are used in each event. For instance, for the event on 24 April 2001, the ranges 22-24, 25-27 and 28-30 were analysed.

5.2 Presentation of data and plots

Figure 5.1 shows the line of sight doppler velocity data obtained from the range set 19-22 on 25 April 2001. The radar operated in the normal scan mode. This event is relatively calm with the doppler velocity fluctuating within ± 500 m/s except for the first few minutes. For the analysis the doppler velocity data were taken from 20 minutes after midnight to 240 minutes after midnight. For this event the solar wind flow speed was about 415 km/s and ACE was 200 R_E from the bow shock. Thus the travel time for the solar wind from ACE to the shock was approximately 52 minutes. The pressure data were taken from about 42 minutes before midnight to about 180 minutes after midnight. It was then converted to a 120 second data vector as described in chapter 4. This is

Event	Scan mode	Range set 1	Range set 2	Range set 3
18/4 2000	high	23-25	26-28	n/a
19/4 2000	high	23-25	26-28	n/a
12/2 2001	normal	13-16	17-20	n/a
24/4 2001	high	22-24	25-27	28-30
25/4 2001	normal	19-22	23-26	n/a
30/4 2001	normal	23-26	27-30	31-34
4/5 2001	normal	19-22	23-26	27-30
5/5 2001	normal	23-26	27-30	n/a
9/6 2001	high	20-22	23-25	26-28
17/9 2001	normal	19-22	23-26	n/a

Table 5.1: Summary of the analysed events.

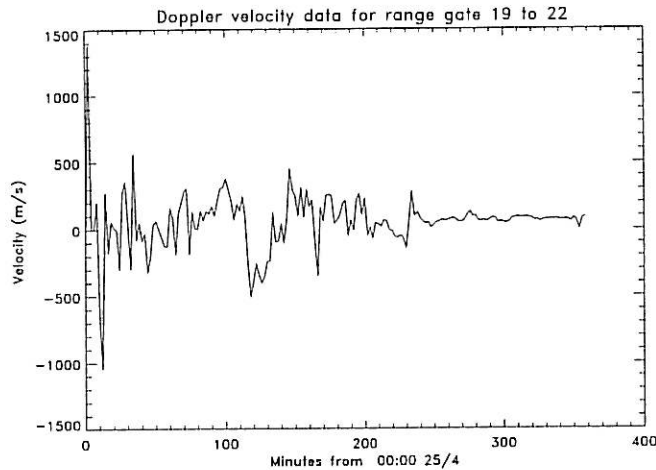


Figure 5.1: Line of sight doppler velocity for beam 4.

plotted in figure 5.2. Since the sample rate is 120 seconds in the normal mode this means that the velocity data vector that was extracted contained 100 data points, equivalent to 200 minutes of data. Figure 5.3 shows the spectrum of the doppler velocity data (dotted line), superimposed is the dynamic pressure of the solar wind (solid line). Notice that the strongest peak in both spectra is located in the same frequency interval (1.2-1.6 mHz).

In order to see if this is just a coincidence or if there indeed is a connection this frequency interval is more closely studied using the method described in chapter four. The result is presented in figures 5.4 and 5.5. Noticeable is the wave packet structure between 20 and 150 minutes in the pressure plot and a similar wave packet structure between 80 and 210 minutes in the velocity plot. This is reflected in the correlation coefficient for the two envelopes displayed in figure 5.6. The correlation coefficient is plotted as a function of lag. The maximum is located at about 64 minutes, which is in agreement with the propagation time from ACE to the location of the FLR. The peak is relatively broad so that there is an uncertainty of about ± 10 minutes in the arrival time. This does not necessarily present a problem since the propagation velocity for the MHD wave is not exactly known. The main interest here is to see if there is a correlation and such details are not of great importance for this analysis. On the other hand, it would be unphysical for the correlation-coefficient to peak at a lag that differs greatly from the propagation time. Such peaks, and they do occur, are here placed on an equal footing with no correlation at all.

For a wave packet the frequency is stable as noted by *Walker et al.*, [1992] and shown in the frequency plots in figure 5.4 and 5.5. The dips and peaks in frequency are often an indication of a new wave packet.

Figure 5.7 to 5.11 shows correlation plots for a representative sample of the studied events. Each column corresponds to a specific range set on a specific

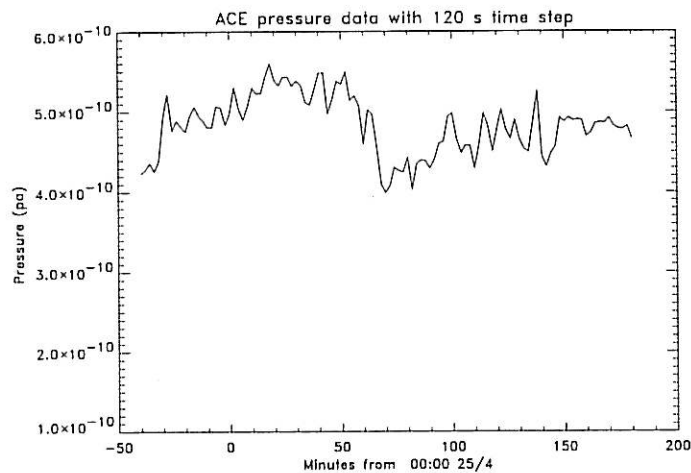


Figure 5.2: The dynamic pressure calculated from solar wind parameters from ACE. The time step for each data point has been changed from 64 seconds to 120 seconds to allow further comparison with radar data.

day. The lowest frequency analysed is at the top and the highest at the bottom. Notice that the scale is not the same in all plots.

One important observation is that for the lowest frequency band in each event, at least eight of the ten plots show a good correlation. This is a really interesting observation since these low frequencies, 0.8-1.2 mHz, are hard to fit into the cavity- or waveguide-model. Also many of the higher frequency bands show high peaks in the correlation coefficient at reasonable time lags, supporting the idea that they are driven by the solar wind. Of course the time lag is strongly dependent on the solar wind speed, but in none of the studied events did it deviate substantially from 400 km/s. Therefore it could be expected that a possible correlation should peak at a lag time around 45 to 65 minutes, and this is also seen in many of the events. Plots from the event on 19 April 2000 are not presented simply because they did not show any correlation at all between the solar wind and the FLRs (i.e., regardless of what range set or what frequency band that was examined no correlation was seen). Why this was the case is further discussed in section 5.3.

The event on 18 April 2000 was especially good with about six hours of consecutive backscatter. Also the radar operated in the high scan mode allowing for an unusually good comparison. The result is that one of the correlation plots show good and the other three show excellent correspondence between the two signals.

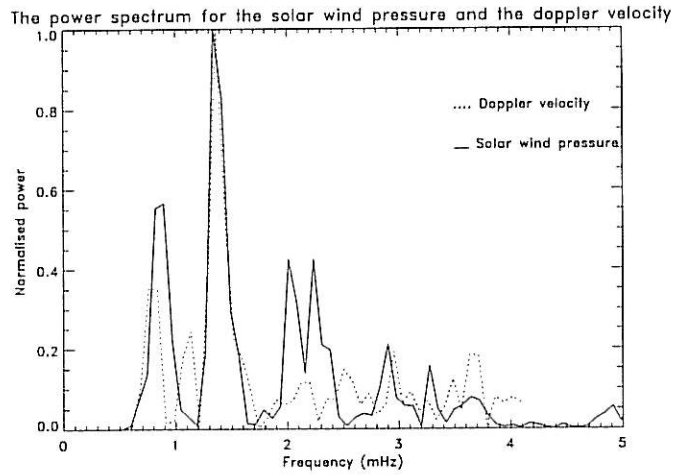


Figure 5.3: Spectra for the event on 25/4 2001 for range set 19-22. Frequencies below 0.5 mHz are filtered out.

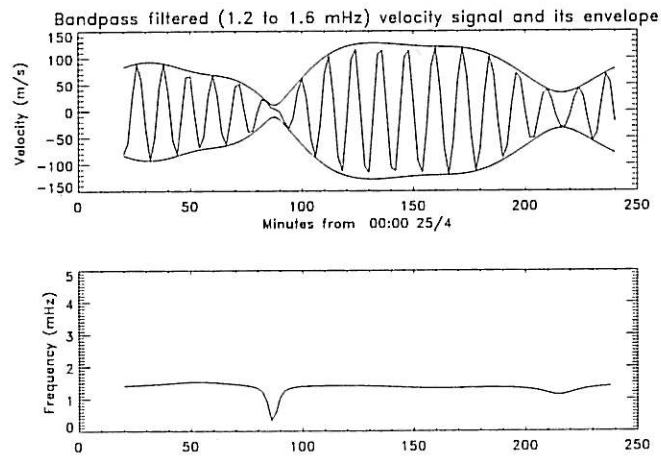


Figure 5.4: Temporal behaviour of the doppler velocity in the 1.2 - 1.6 mHz frequency band. The lower plot is the instantaneous frequency extracted from the analytic signal.

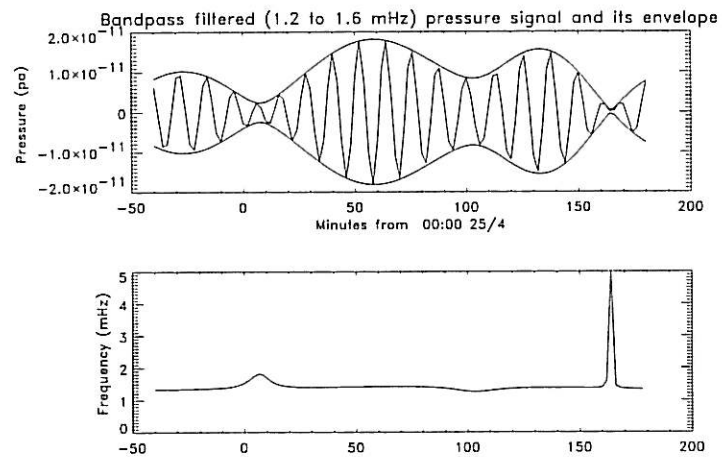


Figure 5.5: Same as figure 5.4 but for the dynamic pressure.

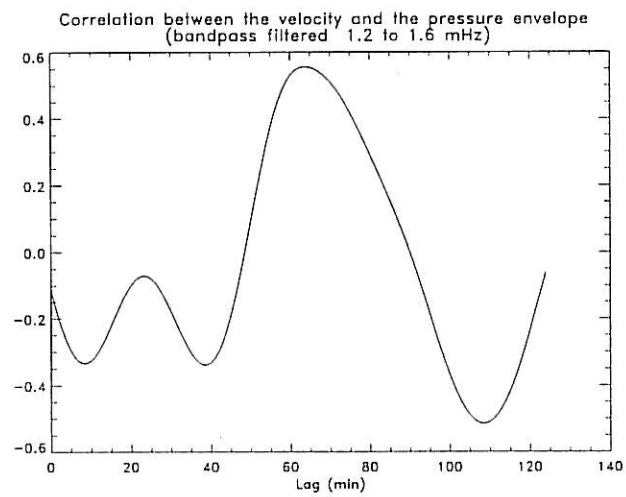
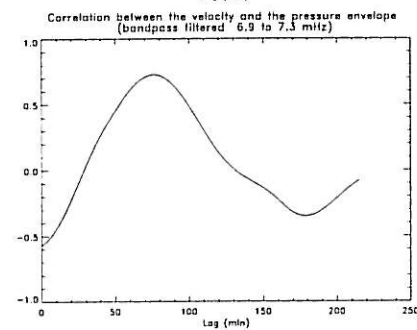
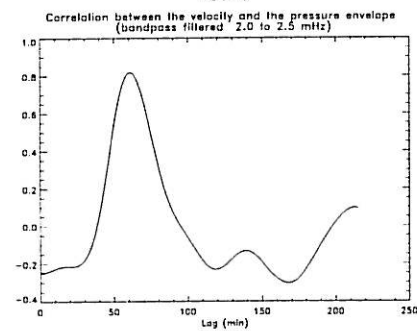
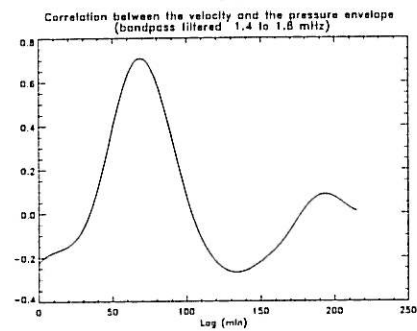
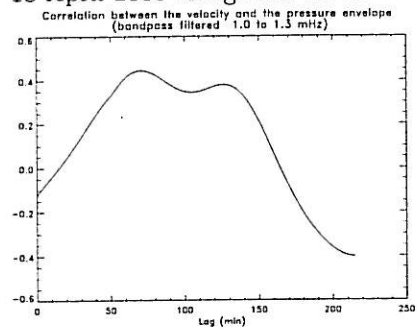


Figure 5.6: Plot of the correlation coefficient between the doppler velocity and dynamic pressure envelope as a function of lag.

18 April 2000 Range set: 26-28



4 May 2001 Range set: 27-30

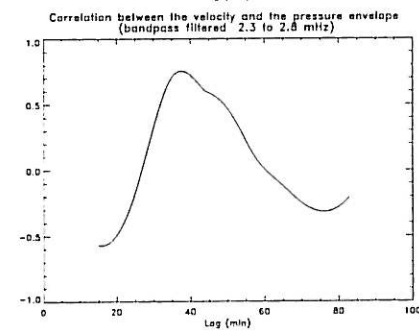
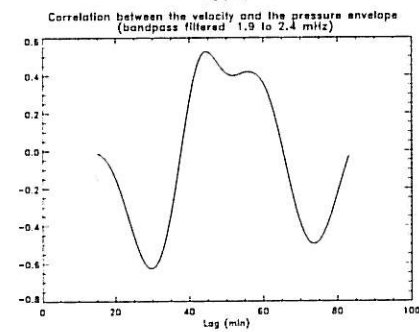
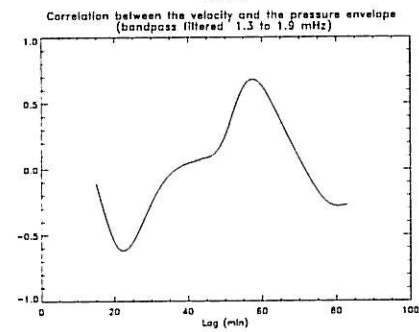
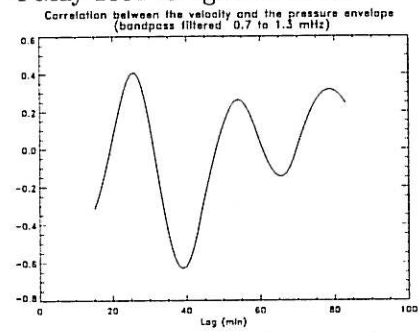
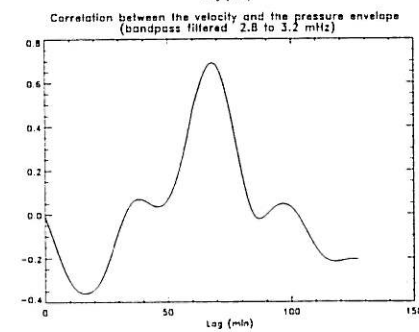
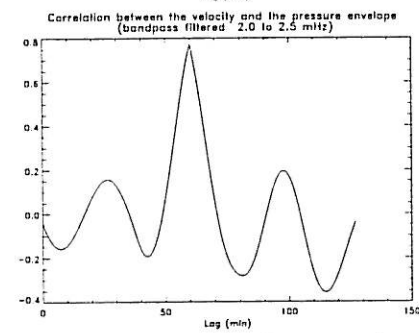
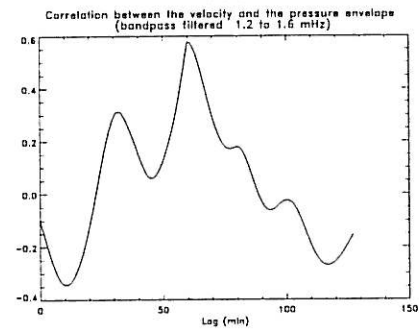
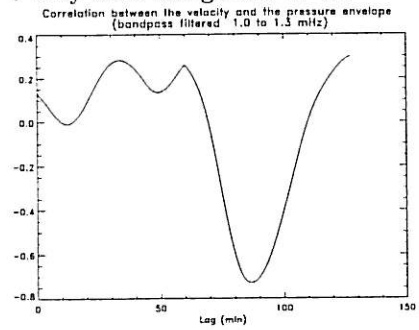


Figure 5.7:

5 May 2001 Range set: 27-30



9 June 2001 Range set: 20-22

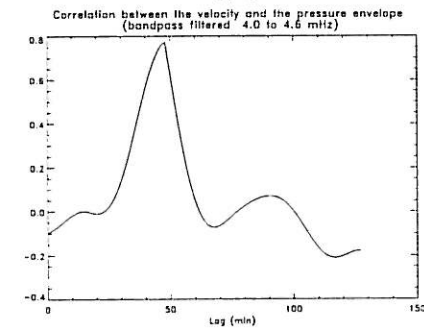
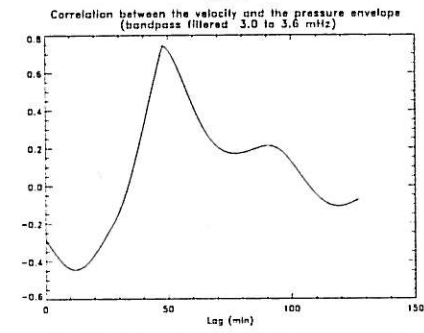
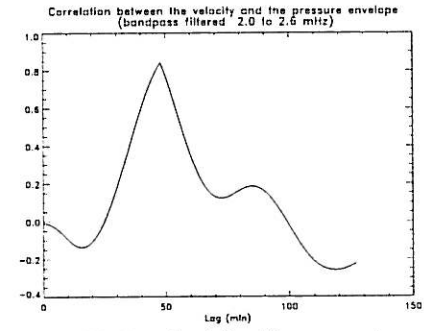
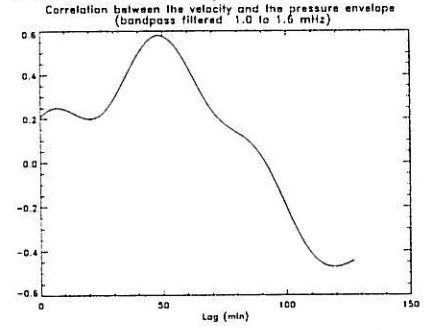
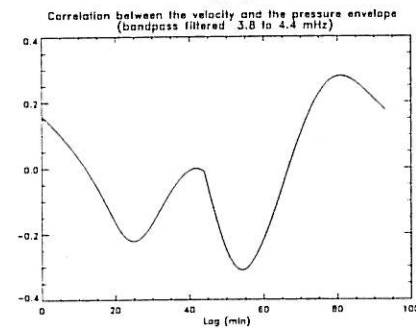
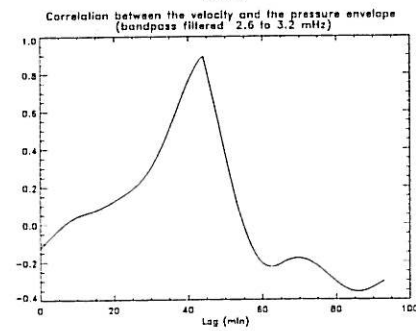
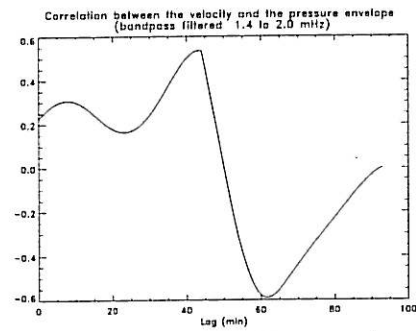
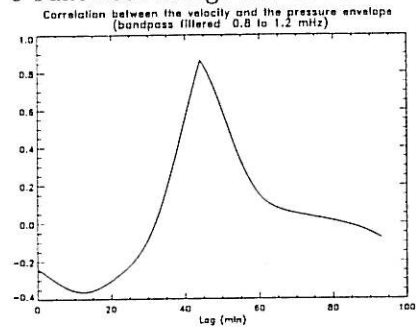


Figure 5.8:

9 June 2001 Range set: 26-28



12 February 2001 Range set: 13-16

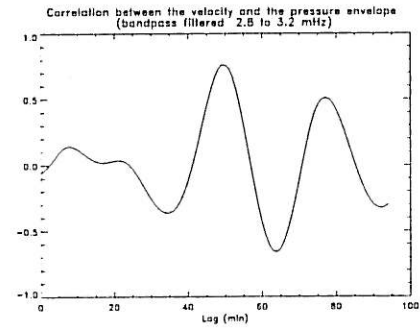
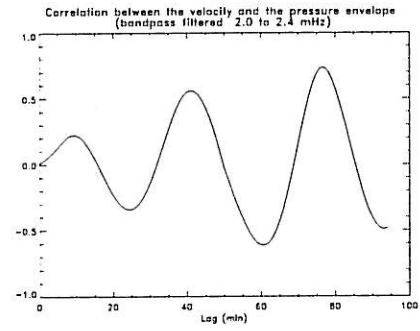
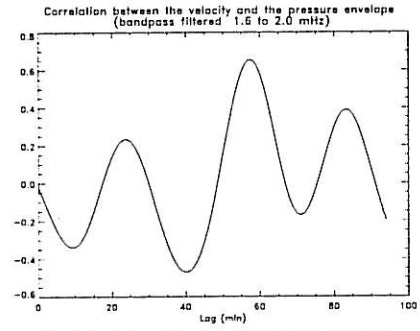
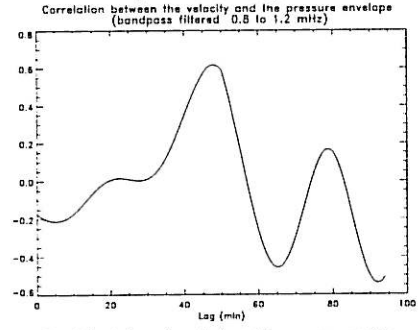
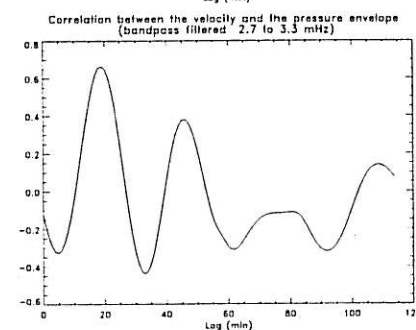
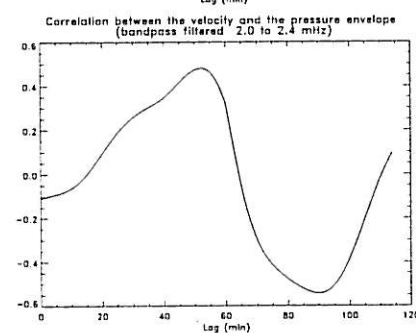
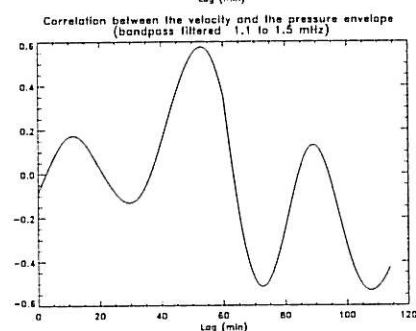
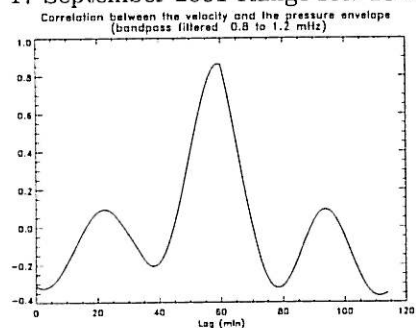


Figure 5.9:

17 September 2001 Range set: 23-26



24 April 2001 Range set: 25-27

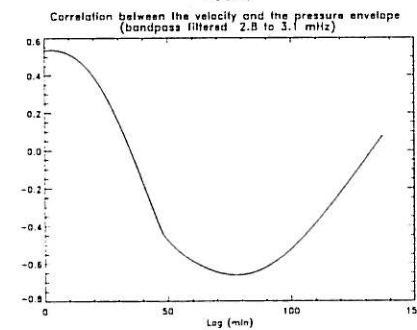
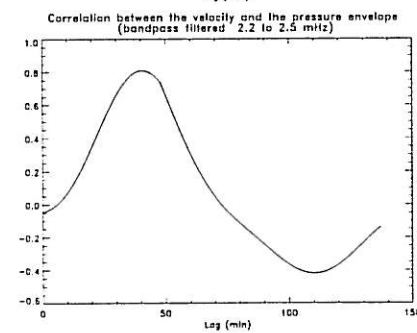
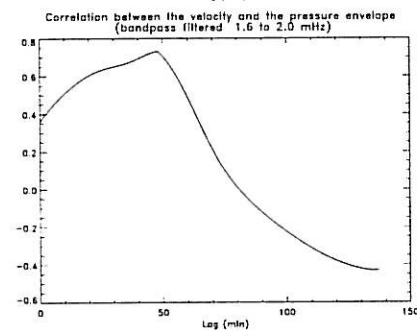
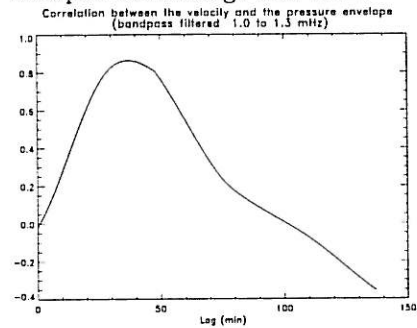
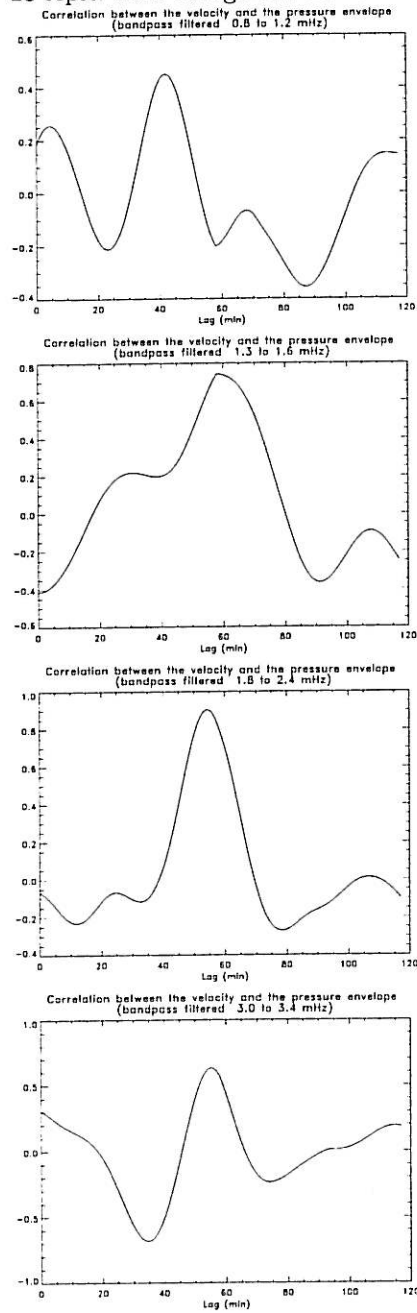


Figure 5.10:

25 April 2001 Range set: 23-26



29 April 2001 Range set: 31-34

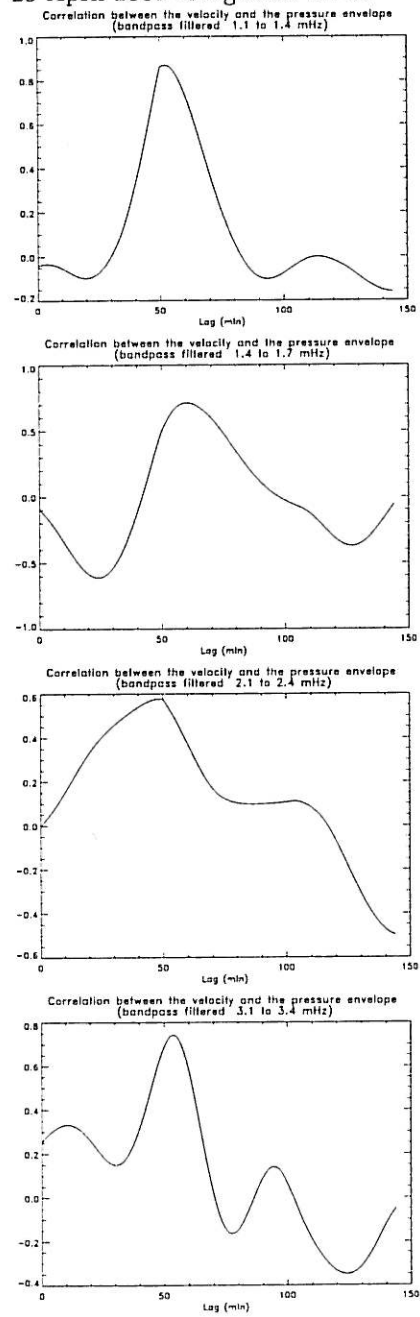


Figure 5.11:

5.3 Some results regarding the spatial structure of the solar wind

It is not clear how well a point measurement far upstream is representative for the solar wind structure arriving at the magnetopause. To resolve this issue in some detail, ACE data have been correlated with data from WIND. On a handful occasions WIND's position has allowed this to be carried out for some different distances, ranging from about $5 R_E$ up to about $120 R_E$.

Between 22:00 08-06-2001 and 06:00 09-06-2001 ACE and WIND were located as shown of figure 5.12. The X coordinate (in GSE) for ACE was about $1.52 \cdot 10^6$ km and $6.37 \cdot 10^5$ km for WIND. The average solar wind velocity in the X direction was 420 km/s. This yields a flow time for the solar wind from ACE to WIND of 35 minutes. The dynamic pressure was calculated and is plotted in figure 5.13. This alignment of ACE and WIND corresponds more or less to two measurement along the solar wind flow. Thus, it can be expected that the two signals should be similar and only time-shifted by the solar wind travel time. This is indeed seen in figure 5.13 where the structure in the upper plot (WIND) is similar to that of the lower plot (ACE) and displaced by about 30 minutes. This is also seen in figure 5.14 where the correlation coefficient between WIND and ACE peaks at about 34 minutes.

Since WIND is located almost directly behind ACE in the flow direction a very high correlation is to be expected. The relatively low correlation coefficient could partially be due to the high and fluctuating sample rate, usually somewhere between 90 and 110 seconds, of the plasma instruments on WIND. The results are nevertheless in good agreement. This is however not the case when WIND has a Y coordinate that differs of about a hundred R_E from ACE. On such occasion no correlation between the two signals is seen. This would suggest that the point measurements made by ACE not always is representative of what later "hits" the magnetopause. So that the complete lack of correlation seen on the 19th April 2000 may be a result of that the signal simply "missed" ACE.

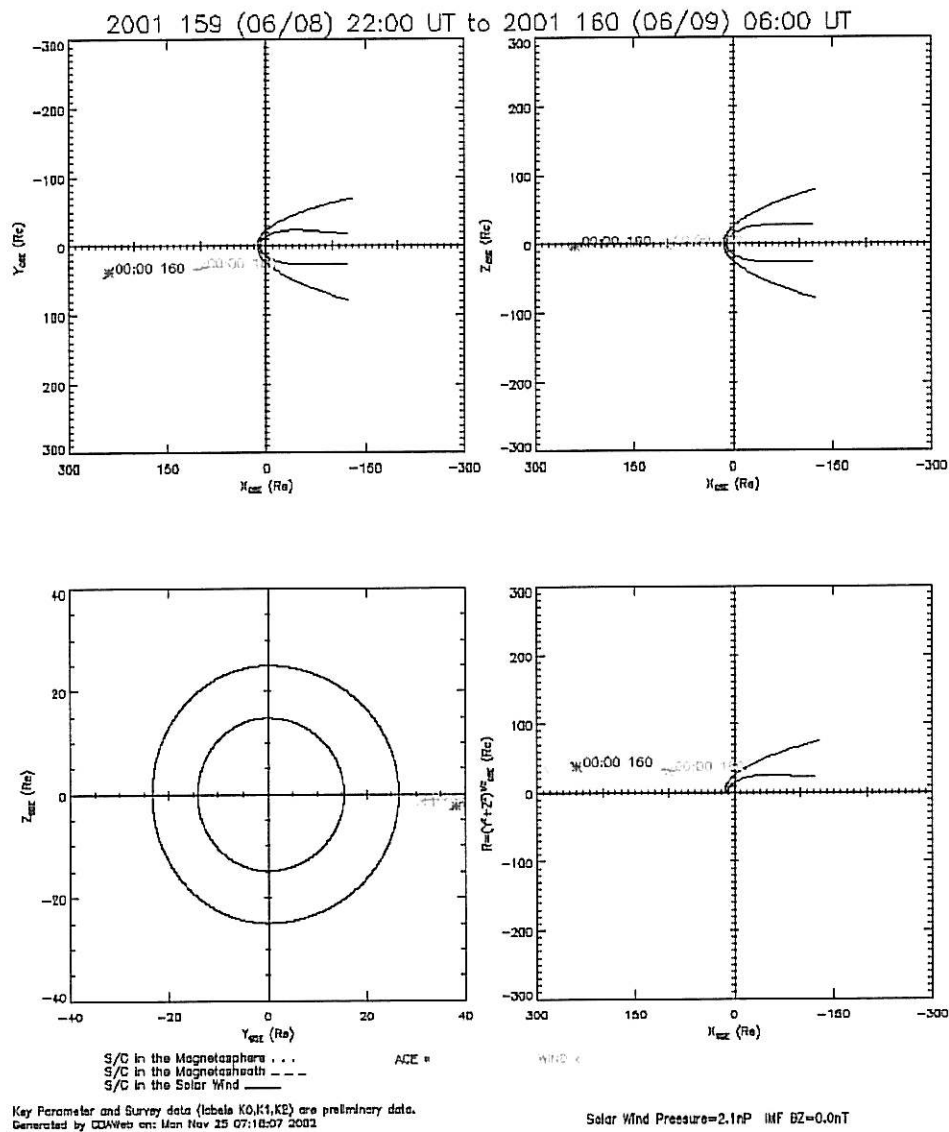


Figure 5.12: The positions of ACE and WIND from 22:00 8/6 2001 to 06:00 9/6 2001 given in GSE coordinates.

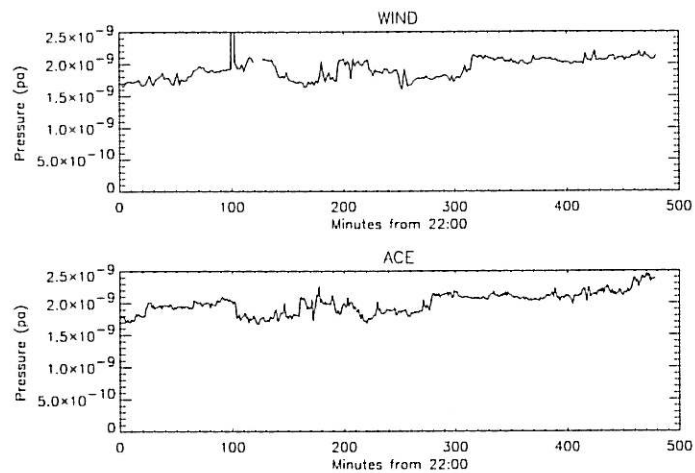


Figure 5.13: Pressure data from WIND and ACE. The sharp peak at about 100 minutes in the upper plot is due to bad data from WIND.

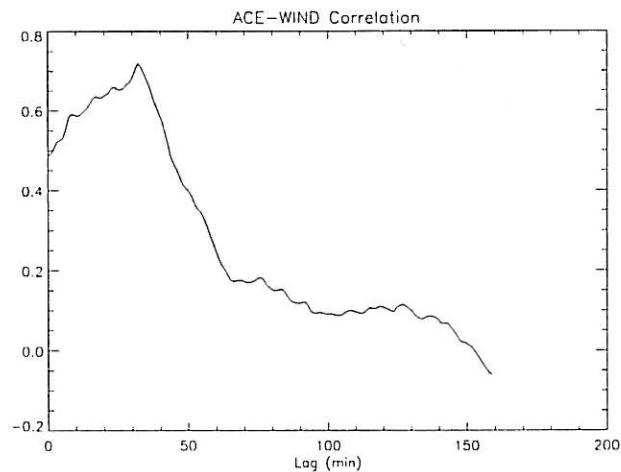


Figure 5.14: Correlation coefficient between the pressure measured by WIND and ACE

Chapter 6

Discussion and Conclusions

6.1 Main conclusions

- In nine of the ten studied events examples of good correlation were found, suggesting that at least some of the Pc-5 pulsation were directly driven by coherent solar wind MHD waves.
- Low frequency Pc-5 pulsation, i.e., 0.8-1.2 mHz, are hard to explain with the cavity/waveguide model. However, in this study these frequencies show very good correlation, much better than other frequencies, with the dynamic pressure.
- The spatial structure of the solar wind seems not to be constant over large distances in the y direction (in GSE coordinates). This could explain why on some occasions no correlation between the dynamic pressure and FLRs is seen.

6.2 Discussion

The conclusion that waves in the solar wind is a driving mechanism for FLRs is supported by the findings of Stephenson and Walker (2002), Prikryl *et al.*, (1998) and Prikryl *et al.*, (2002). This gives a plausible explanation of the low frequency pulsations observed, but hard to reconcile with the cavity/waveguide model. They could simply be driven by a source located outside of the magnetosphere and with the magnetospheric cavity acting like an optical thin film or filter as suggested by Walker (2002). It also gives some answer to why certain frequencies appear more often than others, although the problem is “moved out” to the solar wind.

In this thesis the first order dynamic pressure of the solar wind has been the main subject of analysis. This means that several other variations in the solar wind, which also could excite FLRs, have been omitted. For instance, Potemra *et al.*, (1989) reports that variations in the solar wind density appears to cause FLRs. It could prove interesting to conduct such an analysis parallel to the one done here.

Frequency dependent delay time in the magnetosphere has been observed by Prikryl *et al.*, (2002). This is not supported by theory and is not seen in this study. It should be noted however that in this study no explicit care has been taken to determine such a delay. It could very well be embodied in the uncertainty in lag time.

A complicating factor that arises when correlating FLRs with solar wind data is that the resonant latitude changes with time [Walker *et al.*, 1992]. This means that although a wave packet incident from the solar wind is driving a FLR the correlation may be lost since the amplitude of the FLR is decreasing at the particular altitude observed.

6.3 Future directions

The question of how well a point measurement (like the one done by ACE) represents the structure of the solar wind incident on the magnetosphere needs to be examined more closely. This could for instance be done with the CLUSTER satellites.

Since the FLRs occur on a global scale an obvious step in further investigations would be to use data from several SuperDARN radars in both hemispheres. Also the use of ground-based magnetometers might be useful, at least as a complement to the radars. A third option for measuring the FLRs would be to use one or several satellites placed somewhere in the magnetosphere where the FLRs occur. A problem with this is the limited spatial coverage. A satellite represents a point measurement whereas the radar can cover a large area (and thus several frequencies) simultaneously. The rapid movement of the satellites would also be a complicating factor.

Other methods of filtering could also be implemented. Pure state filtering is used by Prikryl *et al.*, (1998) and would be a complement to the filtering technique used here.

Bibliography

- [1] Chen, L., and A. Hasegawa, A theory of long-period magnetic pulsation, 1, Steady state excitation of field line resonance, *J. Geophys. Res.*, 79, 1024-1032, 1974.
- [2] Greenwald, R. A., K. B. Baker, J. R. Dudeney, M. Pinnock, T. B. Jones, E. C. Thomas, J.-C. Villain, J.-C. Cerrisier, C. Senior, C. Hanuise, R. D. Hunsucker, G. Sofko, J. Koehler, E. Nielsen, R. Pellinen, A. D. M. Walker, N. Sato, and H. Yamagishi, DARN/SUPERDARN A global view of the dynamics of highlatitude convection, *Space Sci. Rev.*, 71, 761-796, 1995.
- [3] Kivelson, M. G., and C. T. Russel, *Introduction to Space Physics*, Cambridge University Press, 1995.
- [4] Potemra, T. A., H. Lühr, L. J. Zanetti, K. Takahashi, R. E. Erlandson, G. T. Marklund, L. P. Block, L. G. Blomberg, and R.P. Lepping, Multisatellite and Ground-Based Observations of Transient ULF Waves, *J. Geophys. Res.*, 94, 2543-2554, 1989.
- [5] Prikryl, P., R.A. Greenwald, G. J. Sofko, J. P. Villain, C. W. S. Ziesolleck, and, E. Friis-Christensen, Solar-wind-driven pulsed magnetic reconnection at the dayside magnetopause, Pc5 compressional oscillations, and field line resonances, *J. Geophys. Res.*, 103, 17,307-17,322, 1998.
- [6] Prikryl, P., G. Provan, K. A. McWilliams, and T.K. Yeoman, Ionospheric cusp flows pulsed by solar wind Alfvén waves, *Ann. Geophysicae*, 20, 161-174, 2002.
- [7] Ruohoniemi, J. M., R. A. Greenwald, K. B. Baker, and J. C. Samson, HF radar observations of Pc5 field line resonances in the midnight/early morning MLT sector, *J. Geophys. Res.*, 96, 15,697-15,710, 1991.
- [8] Samson, J. C., R. A. Greenwald, J. M. Ruohoniemi, T. J. Hughes, and D. D. Wallis, Magnetometer and radar observations of magnetohydrodynamic cavity modes in the earths magnetosphere, *Can. J. Phys.*, 69, 929-937, 1991.
- [9] Southwood, D. J., Some features of field line resonances in the magnetosphere, *Planet. Space Sci.*, 22, 483-491, 1974.
- [10] Stephenson, J. A. E., and A. D. M. Walker, HF radar observations of Pc5 ULF pulsations driven by the solar wind, *Geophys. Res. Lett.*, 29, 1029/2001GL014291, 2002.

- [11] Walker A. D. M., J. M. Ruohoniemi, K. B. Baker, R. A. Greenwald, and J. C. Samson, Spatial and temporal behavior of ULF pulsations observed by the Goose Bay HF radar, *J. Geophys. Res.*, 97, 12,187-12,202, 1992.
- [12] Walker A. D. M., Excitation of Field Line Resonances by MHD Waves Originating in the Solar Wind, *J. Geophys. Res.*, 107(A12), 1481, doi:10.1029/2001JA009188, 2002.

